International Journal of Polymer Analysis and Characterization

ISSN: (Print) (Online) Journal homepage: https://www.tandfonline.com/loi/gpac20

Development of a poly(urethane-malonic-esteramide) coating from corn oil and carbon nanotubes for corrosion resistant applications

Manawwer Alam , Naser M. Alandis , Javed Alam , Naushad Ahmad & Mohammad Asif Alam

To cite this article: Manawwer Alam , Naser M. Alandis , Javed Alam , Naushad Ahmad & Mohammad Asif Alam (2021) Development of a poly(urethane-malonic-esteramide) coating from corn oil and carbon nanotubes for corrosion resistant applications, International Journal of Polymer Analysis and Characterization, 26:2, 111-129, DOI: 10.1080/1023666X.2020.1858666

To link to this article: https://doi.org/10.1080/1023666X.2020.1858666

INTERNATIONAL JOURNAL OF POLYMER ANALYSIS AND CHARACTERIZATION
2021, VOL. 26, NO. 2, 111–129
https://doi.org/10.1080/1023666X.2020.1858666

Taylor & Francis
Taylor & Francis Group

Development of a poly(urethane-malonic-esteramide) coating from corn oil and carbon nanotubes for corrosion resistant applications

Manawwer Alam[a], Naser M. Alandis[a], Javed Alam[b], Naushad Ahmad[a], and Mohammad Asif Alam[b,c]

[a]Department of Chemistry, College of Science, King Saud University, Riyadh, Saudi Arabia; [b]Center of Excellence in Engineering Materials, King Saud University, Riyadh, Saudi Arabia; [c]King Abdullah Institute for Nanotechnology, King Saud University, Riyadh, Saudi Arabia

ABSTRACT

Poly(urethane-malonic-esteramide) (PUMEA), a novel resin synthesized from corn oil-based fatty amide, malonic acid, and isophorone diisocynate, was modified by introducing different amounts of multi-walled carbon nanotubes (MWCNTs) into the polymer matrix and cured at room temperature. The chemical structure and surface morphology were characterized by Fourier-transform infrared spectroscopy, nuclear magnetic resonance, and field emission scanning electron microscopy, and thermal analysis was carried out by thermogravimetric analysis and differential scanning calorimetry. The PUMEA/MWCNTs composites were coated on mild steel panel and cured at room temperature. Hydrophobicity and physico-mechanical properties of the coatings were extracted by measuring contact angle, scratch and pencil hardness, bending, cross-hatch adhesion, impact, and gloss. The corrosion resistance was proved measuring the potentiodynamic polarization and electrochemical impedance of a PUMEA-coated mild steel panel immersed in a 3.5 wt% NaCl solution for 40 days. Thermal studies revealed that the PUMEA coating can be safely used up to 250 °C.

ARTICLE HISTORY
Received 24 September 2020
Accepted 27 November 2020

KEYWORDS
Corn oil; polyurethane; MWCNT; corrosion

Introduction

Polymer coatings are the best corrosion protection for mild steel. Among polymer coatings, different materials are commonly used, including alkyd, polyesteramide, polyetheramide, polyester,[1,2] polyurethane,[3,4] polyepoxy,[5] nanoparticle-containing polymeric materials, and polymer composites.[6,7] Polyurethane is an important class of polymers commonly used in furniture, footwear, and the automotive industry.[8] Despite its wide range of applications, the production of polyurethane presently depends on petroleum-based polyols.[9] Recently, because of environmental and economic concerns, the preparation of polyols from sustainable resources such as lignin, vegetable oil, starch, cellulose, and chitosan has received increasing attention.[4,10,11] Developing sustainable polyols from vegetable oil-based materials is a step toward a solid and durable production of polymer coatings characterized by intrinsic renewability, easy modifiability, and relatively low cost.[12,13] In the preparation of sustainable polymeric materials, different vegetable oils have been used as raw materials, including soybean, palm, rapeseed, castor, linseed, pongamia, and sunflower oil.[13,14] However, vegetable oil-based polyesteramide, polyetheramide, polyepoxy,

CONTACT Manawwer Alam maalam@ksu.edu.sa, malamiitd@gmail.com Department of Chemistry, College of Science, King Saud University, P.O. Box 2455, Riyadh 11451, Saudi Arabia.

and polyurethane have poor physico-mechanical properties and thermal stability.[15] To improve the properties of vegetable oil-based polymeric materials, different ceramic particles are used, such as CeO_2,[16] SiO_2,[17–19] Al_2O_3,[20] ZnO, TiO_2,[19,21,22] $CaCO_3$, and multi-walled carbon nanotubes (MWCNTs).[17,23–29]

Malonic (propanedioic) acid is an aliphatic dicarboxylic acid used as a precursor in biosynthesis. In particular, malonic acid is used in the synthesis of cinnamic acid and, in the pharmaceutical and food industries, in the preparation of fragrances, adhesives, lubricants, polyamides, polyesters, and biodegradable thermoplastics.[29–33] Introducing nanofillers into polymeric organic coatings can improve their barrier performance by decreasing their porosity and reducing the diffusion path of deleterious species.[34–36] Thus, polymeric coatings containing MWCNTs are expected to have significant barrier performance, providing protection from corrosion, reducing blistering and delamination, and improving the physico-mechanical properties of mild steel.[23,36–40]

This study focuses on the use of corn oil-fatty amide diol for developing renewable resource-based poly (urethane-malonic-esteramide) (PUMEA). PUMEA has been sparsely studied in research. It is obtained from treating polyesteramide, in turn obtained from the reaction of corn oil (58–62% linoleic acid) in fatty amide diol with malonic acid, with isophorone diisocynate (IPDI). To further improve the mechanical and thermal properties of PUMEA, MWCNTs were introduced to obtain a PUMEA/MWCNTs nanocomposite. As a polymeric composite coating, the PUMEA/MWCNTs nanocomposite has not been previously investigated in the development of corrosion-resistant coatings. Additionally, MWCNTs are used to prepare a PUMEA/MWCNTs nanocomposite for corrosion protection for the first time. The PUMEA and PUMEA/MWCNTs composites prepared are characterized by Fourier-transform infrared spectroscopy (FTIR), nuclear magnetic resonance (NMR), field emission scanning electron microscopy (FESEM), and by measuring contact angle, potentiodynamic polarization, and electrochemical impedance.

Experimental methods

Materials

Corn oil (Afia International Company, Jeddah, Saudi Arabia), malonic acid (Sigma Aldrich, USA), isophorone diisocynate (IPDI) (Acros Organic, USA), diethanolamine (Riedel-deHaen, Germany), methanol, toluene, sodium (BDH Chemicals, Ltd. Poole, England), and MWCNTs (Nanocyl®-7000, Nanocyl Korea Ltd., Seoul, South Korea; average diameter: 9.5 nm, length: 1.5 µm, purity > 99 wt%) were used to synthesize PUMEA and PUMEA/MWCNTs nanocomposites.

Synthesis of N,N-bis(2-hydroxyethyl) corn oil fatty amide

N,N-bis(2-hydroxyethyl) corn oil fatty amide (HECA) was synthesized following the previously published recipe.[41]

Synthesis of malonic polyesteramide

HECA (0.1 mol) and malonic acid (0.08 mol) were dissolved in toluene and placed in a four-neck round-bottomed flask equipped with a Dean-Stark trap, nitrogen inlet tube, thermometer, and magnetic stirrer. The reactants were heated to 150 °C and stirred until the expected amount of water was stored in the Dean-Stark trap. The reaction was monitored by thin layer chromatography (TLC) and by measuring the acid value. After the reaction, the solvent was evaporated in a rotary vacuum evaporator under reduced pressure to obtain malonic polyesteramide (MPEA).[41]

Synthesis of poly(urethane-malonic-esteramide)

MPEA and IPDI (25 wt%, 30 wt%, 35 wt%, 40 wt%, and 45 wt%) were dissolved in toluene and placed in a round-bottomed flask equipped with a thermometer, condenser, nitrogen inlet tube, and magnetic stirrer. The reaction was carried out at 110 °C under stirring and monitored by TLC and by measuring the hydroxyl value. The solvent was evaporated in a rotary vacuum evaporator under reduced pressure to obtain PUMEA.

Synthesis of poly(urethane-malonic-esteramide) with multi-walled carbon nanotubes

To synthesize the PUMEA/MWCNTs nanocomposite, PUMEA prepared with 40 wt% IPDI was loaded with 0.4 wt%, 0.6 wt%, 0.8 wt%, and 1.0 wt% MWCNTs and mixing with mechanical mixer (Dispers Master, Sheen Instruments. Ltd., UK) at 3000 rpm for 1 h. After complete mixing, sonication was performed at 55 °C for 1 h before the urethane reaction to obtain PUMEA-0.4, PUMEA-0.6, PUMEA −0.8, and PUMEA −1.0, respectively, following the same procedure used for the preparation of PUMEA.

Characterization

FTIR spectra of MPEA and PUMEA were taken on FTIR spectrophotometer (Spectrum 100, PerkinElmer, USA) using NaCl window. ^{1}H and ^{13}C NMR spectra were recorded by a Jeol DPX400MHz spectrometer (Japan) using deuterated dimethyl sulfoxide (DMSO-d_6) as solvent and tetramethylsilane (TMS) as internal standard. Thermal analysis was performed by thermogravimetric analysis (TGA) and differential scanning calorimetry (DSC) (TGA/DSC1, Mettler Toledo AG, Analytical CH-8603, Schwerzenbach, Switzerland) in nitrogen atmosphere. In DSC, around 2–3 mg sample was kept in an aluminum pan and sealed with cover and the sample was run from 25 °C to 400 °C with heating rate 10 °C/min and nitrogen flow (50 ml/min). In TGA, 4–5 mg of sample was kept in alumina crucible with cover, and the sample was run from 25 °C to 600 °C with heating rate 10 °C/min and nitrogen flow (50 ml/min). The morphology was studied by SEM (JED-2200 Series, Jeol, Japan). PUMEA coated sample was sputter-coated with gold prior to surveillance under the microscope and operated at 15 kV.

Coatings of PUMEA were prepared by application of the prepared resin on mild steel panels of standard sizes. The mild steel panels were first cleaned with silicon carbide paper and degreased by alcohol and acetone, prior to application of PUMEA coatings over these. PUMEA, PUMEA-0.4, PUMEA-0.6, PUMEA −0.8, and PUMEA −1.0 resins were dissolved in 40% solution of toluene and applied by brush technique on cleaned and degreased mild steel panels. PUMEA-coated panels were dried for 5 min and hardened for 15 days at 27 °C. After 15 days, the curing reaction was completed, and the panels were subjected to physico-mechanical and corrosion tests. Physico-mechanical properties of PUMEA coated mild steel panels were observed using impact resistance (IS: 101 part 5 sec 3, 1988), scratch hardness (BS 3900), crosshatch adhesion (ASTM D3359-02), conical mandrel bend (ASTM D3281-84), and pencil hardness test (ASTM D3363) using a Wolff–Wilborn tester (Sheen Instruments, England). The thickness and gloss of the PUMEA coatings were also measured using an Elcometer coating thickness gauge (Model 456; Elcometer Instruments, Manchester, UK) and a glossmeter (KSJ MG6-F1, KSJ Photoelectrical Instruments Co., Ltd. Quanzhou, China), respectively. The hydrophobicity of PUMEA was observed using distilled water drop (3 μL) on a coated panel and estimated from contact angle measurements using a CAM 200 Attention goniometer. Potentiodynamic polarization (PDP) and electrochemical impedance spectroscopy (EIS) measurements were performed in a three-electrode system at ambient temperature in a corrosive 3.5 wt% NaCl solution, using a PUMEA-0.8-coated mild steel sample as the working electrode, a platinum counter-electrode, a KCl-filled silver

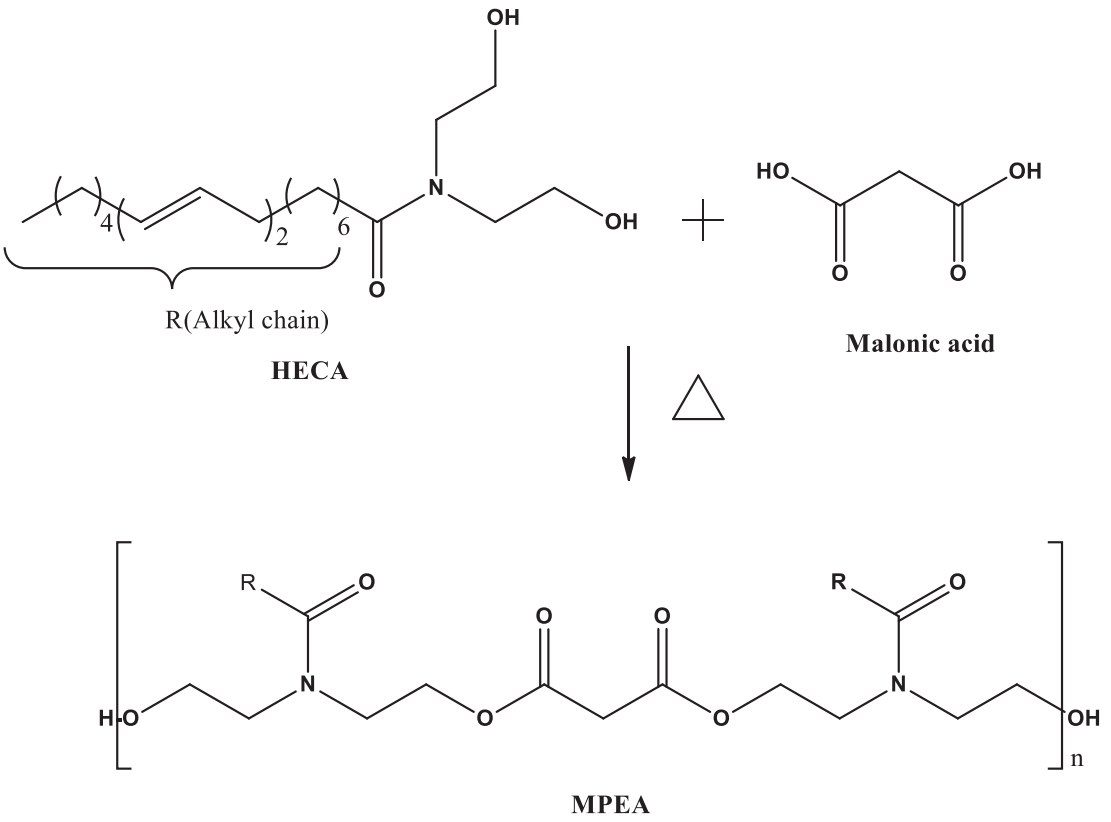

Scheme 1. Synthesis of MPEA.

reference electrode, and an Autolab potentiostat/galvanostat (PGSTAT204-FRA32) with the NOVA 2.1 software (Metrohom Autolab B.V. Kanaalweg 29-G, 3526 KM, Utrecht, The Netherlands). The surface area of the PUMEA-0.8-coated sample exposed was fixed to 1.0 cm^2 using a PortHoles electrochemical sample mask. The PDP (Tafel) curve was obtained at a scanning rate of 10 mV/s in the potential range ±250 mV with respect to the open circuit potential. The EIS measurements were carried out in the 1–10^5 Hz frequency range, with an amplitude of the sinusoidal voltage of 10 mV. The impedance data were analyzed and fitted with the NOVA 2.1 software. Each corrosion test on PUMEA-0.8-coated mild steel was repeated three times to ensure reproducibility.

Results and discussion

Scheme 1 and 2 display the synthesis of MPEA and PUMEA. MPEA was obtained from the reaction of HECA and malonic acid. The free hydroxyl groups of MPEA reacted with IPDI to obtain PUMEA, and MWCNTs were added in different weights to obtain a sequence of nanocomposites with increasing MWCNT content. The structure of MPEA and PUMEA was characterized by FTIR and NMR.

Spectral analysis

FTIR (cm^{-1}), MPEA: 3390.58 (OH); 1740.23 (C=O, ester); 1625.86 (C=O, amide); 3008.20 (chain unsaturation); 2925.72 (CH_2 stretching (str.) asymmetrical); 2854.67 (CH_2 str.

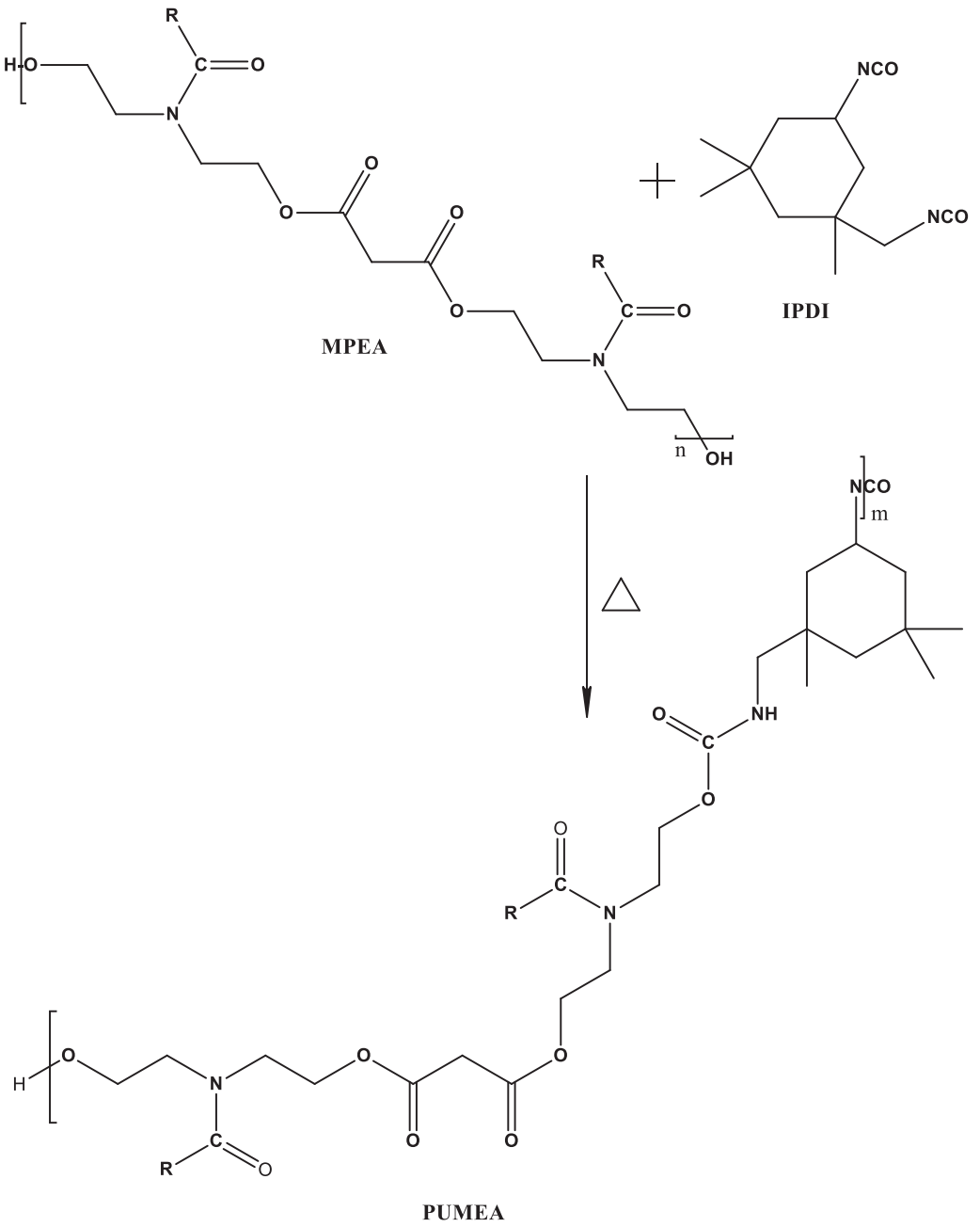

Scheme 2. Synthesis of PUMEA.

symmetrical); 1465.63 (C–N, str.); 1172.18, 1053.10 (–C(CO)O–C–, stretching); 859.54, 722.66, 607.86 (CH, bending) (Figure 1). **PUMEA:** 3221.06 (NH, str.); 2256.21 (free NCO); 1723.36 (C=O, urethane, ester); 1633.80 (C=O, amide); 1464.11 (CN, stretching); 1365.39, 1305.52, 865.76 (ring of IPDI); 774.32 (NH, bending) (Figure 1).

^{1}H NMR (DMSO-d_6, δ), MPEA: 0.807–0.831 (–C**H**$_3$); 1.207 (–C**H**$_2$–); 1.464 (–CO–CH$_2$–C**H**$_2$–); 1.994 (–C**H**$_2$–CH=CH–); 2.263 (–CO–C**H**$_2$–); 2.689–2.704 (–CH =CH–C**H**$_2$–CH=CH–); 3.021 (–CO–C**H**$_2$–CO–); 3.305 (>N–C**H**$_2$–CH$_2$–OH); 3.439–3.452 (–C**H**$_2$OH > NC**H**$_2$–CH$_2$–O–CO–);

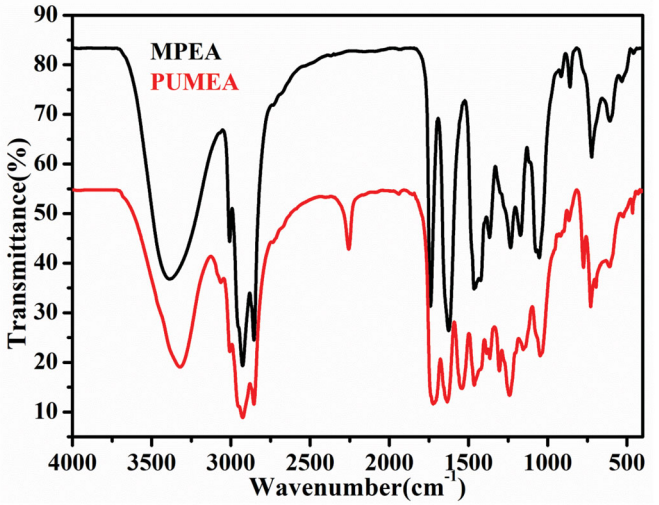

Figure 1. FTIR spectra of MPEA and PUMEA.

4.049–4.060 (–C**H**$_2$–O–CO–CH$_2$–); 4.725–4.755 (CH$_2$–CH$_2$–O**H**); 5.260–5.283 (–C**H**=C**H**–) (Figure 2). **PUMEA:** 7.954 (N**H**, urethane); 4.151 (–**C**H$_2$–CONH); 1.220 (NH–C**H**$_2$-attached to cyclic ring); 3.302 (cyclic-C**H**–NCO); 1.466 (C**H**$_2$, cyclic); 0.967 (–C**H**$_3$ attached cyclic ring) (Figure 3).

^{13}C NMR (DMSO-d$_6$, δ), MPEA: 13.727–13.813 (–**C**H$_3$); 20.052 (–**C**H$_2$–CH$_3$); 22.034 (–CO–**C**H$_2$–); 26.642 (–**C**H$_2$–CH=CH–); 28.08–29.199 (=CH–**C**H$_2$–CH$_2$); 44.301 (–CO –**C**H$_2$–CO–);48.161 (>N–**C**H$_2$–CH$_2$–OH); 51.490 (>N–**C**H$_2$–CH$_2$–O–CO–); 58.891 (–**C**H$_2$–OH); 59.082 (>N–CH$_2$–**C**H$_2$–O–CO–); 127.596–129.609 (–**C**H=**C**H–); 169.851–170.261 (**C**O, ester); 171.997–172.569 (>**C**O, amide) (Figure 4). **PUMEA:** 157.543 (**C**ONH); 155.240 (free N**C**O); 66.342 (–**C**H$_2$CONH); 48.761 (>N–**C**H$_2$–CH$_2$–CONH); 20.783–38.012 (**C,** cyclic) (Figure 5).

Morphological observation

The FESEM images of Figure 6A,B display the cylindrical structure of MWCNTs in two magnifications, respectively, 1 µm and 100 nm. Figure 6C and D show FESEM images of 0.4 wt% MWCNTs uniformly dispersed in the PUMEA matrix without conglomeration. Thus, MWCNTs provide wettability to the PUMEA matrix.[42,43] Generally, it is assumed that the interaction between individual MWCNTs with large surface area is van der Waals' forces of attraction; whereas between MWCNTs and PUMEA good interfacial adhesion is responsible for better dispersion of MWCNTs in PUMEA matrix. Additionally, we observed that the PUMEA-0.8 coating is the one best adhering to the mild steel substrate, improving its physico-mechanical properties. Figure 8 The SEM image (Figure 7) of PUMEA-0.8 coating were taken after immersion in 3.5 wt% NaCl solution, which showed the coating was unaffected with salt deposition (except some white spots) on the surface and there was a slight loss in gloss, however the ions could not penetrate through PUMEA-0.8 coating, which did not show any dissolution.

Contact angle measurements

Figure 8 shows images of water drops on the surface of PUMEA and MWCNTs-modified PUMEA, displaying the evolution of the contact angle from PUMEA to PUMEA-1.0 composites for increasing contents of MWCNTs. The contact angle of PUMEA, PUMEA-0.4, PUMEA-0.6, PUMEA-0.8, and PUMEA-1.0 was respectively 84°, 104°, 107°, 109°, and 110°. As can be seen, the values of the contact angle values increased in MWCNTs-modified PUMEA. This is because

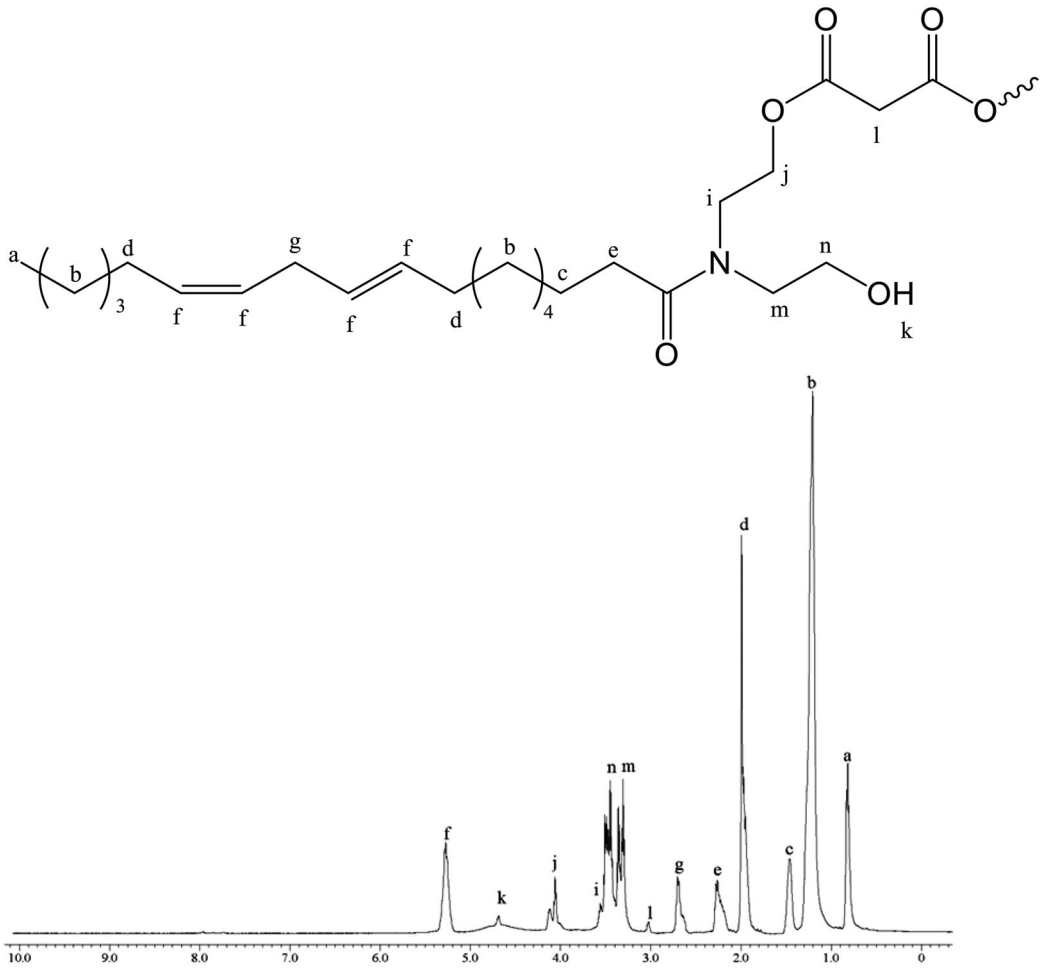

Figure 2. ^{1}H NMR spectra of MPEA.

of its lower surface energy with respect to PUMEA and because of the hydrophobic nature of MWCNTs. The different interfacial wettability in MWCNTs-modified and PUMEA coatings is attributed to a change in polarity of the coating surface in presence of the MWCNTs. The greater hydrophobicity of the MWCNTs-modified coatings means that these materials can be applied as anti-corrosion coatings.[44,45]

Physico-mechanical characterization

The PUMEA, PUMEA-0.4, PUMEA-0.6, PUMEA-0.8, and PUMEA-1.0 coatings were dried at room temperature. The thickness of the coating was found to be 170 ± 5 µm. The scratch hardness values of PUMEA, PUMEA-0.4, PUMEA-0.6, PUMEA-0.8, and PUMEA-1.0 were 1.8 kg, 2.0 kg, 2.5 kg, 2.8 kg, and 2.7 kg, respectively, beyond which the scratch hardness deteriorated. The pencil hardness values were, respectively, measured 2B, 2H, 4H, 6H, and 5H, deteriorating beyond PUMEA-0.8, i.e., beyond a 0.4 wt% loading of MWCNTs in the PUMEA resin. The gloss values at 45° were found to be 68 (PUMEA), 72 (PUMEA-0.4), 75 (PUMEA-0.6), 85 (PUMEA-0.8), and 90 (PUMEA-1.0). The PUMEA and MWCNT-modified PUMEA coatings displayed good bending (1/8 inch), impact resistance (150 lb/inch), and cross-hatch (100%) results. These results for

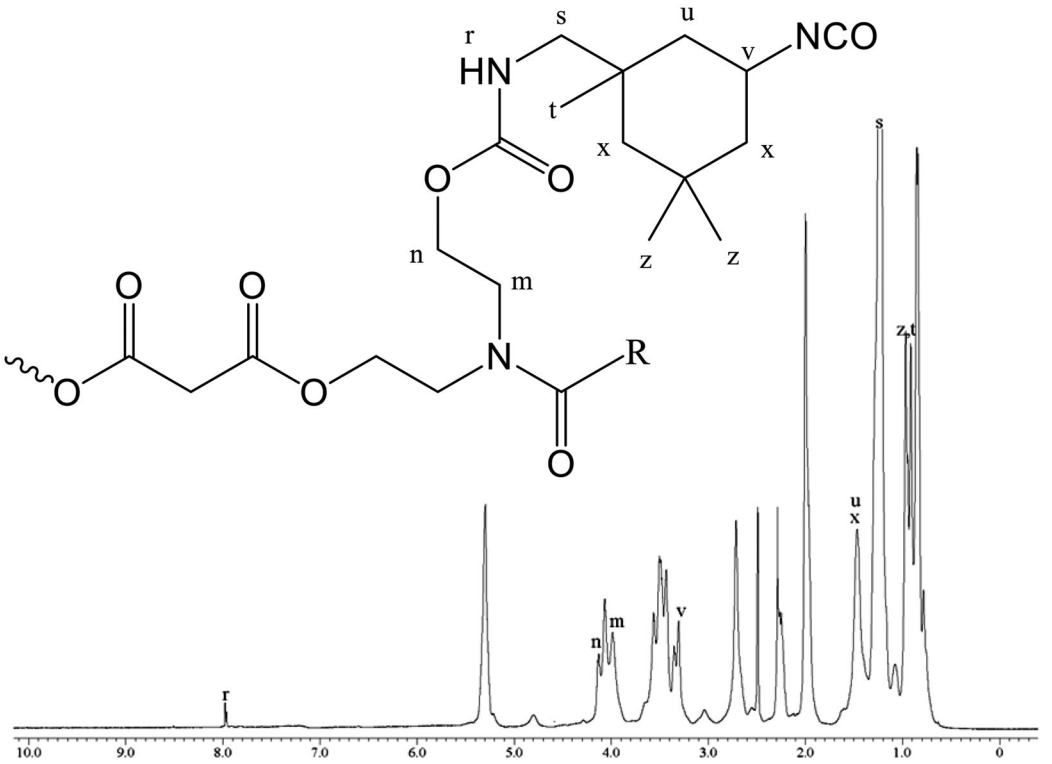

Figure 3. ^{1}H NMR spectra of PUMEA.

MWCNTs-modified PUMEA are attributed to an increased crosslinking density and rigidity provided by the carbon nanomaterials. However, when the content of MWCNTs was equal to or over 1.0 wt%, the physico-mechanical properties decreased dramatically. This may be because of an insufficient interaction between PUMEA and carbon and because the interface energy and the large surface area of the MWCNTs impede their homogeneous distribution in the PUMEA coatings.[46]

Polarization measurements

Polarization curves are measured for PUMEA-0.8 in a 3.5% NaCl aqueous solution, and the electrochemical parameters extracted from them are reported in Table 1. Figure 9 shows the polarization curves measured at different immersion times (4–40 days) with 4-day intervals. For all immersion times, both oxidation and reduction branches are clearly observed in the Tafel curves, and the redox reactions occurring in the two branches can be related to corrosion of the metal surfaces and passivation of the PUMEA-0.8 coating, respectively. To verify this, the Tafel region is extrapolated from the cathodic and anodic polarization curves and used to compute the corrosion rate and reduction behavior of the PUMEA-0.8 coating. The Tafel curves shown in Figure 9 have been calculated in terms of the E_{corr} and I_{corr} parameters reported in Table 1. The E_{corr} parameter decreases continuously from −0.257 V to −0.593 V for increasing immersion times (from 4 to 40 days), whereas I_{corr} increases from 6.554 E-08 to 1.166 E-06. Meanwhile, the corrosion rate increases and the polarization resistance decreases, indicating that the PUMEA-0.8 coating is corrosion-resistant. After 32 days, the corrosion rate rapidly increases, indicating that corrosive ions penetrate the PUMEA-0.8 coating. Before this, no effect of corrosion was observed, because the PUMEA-0.8 coating is hydrophobic and well-adhered, having a compact, uniform, and

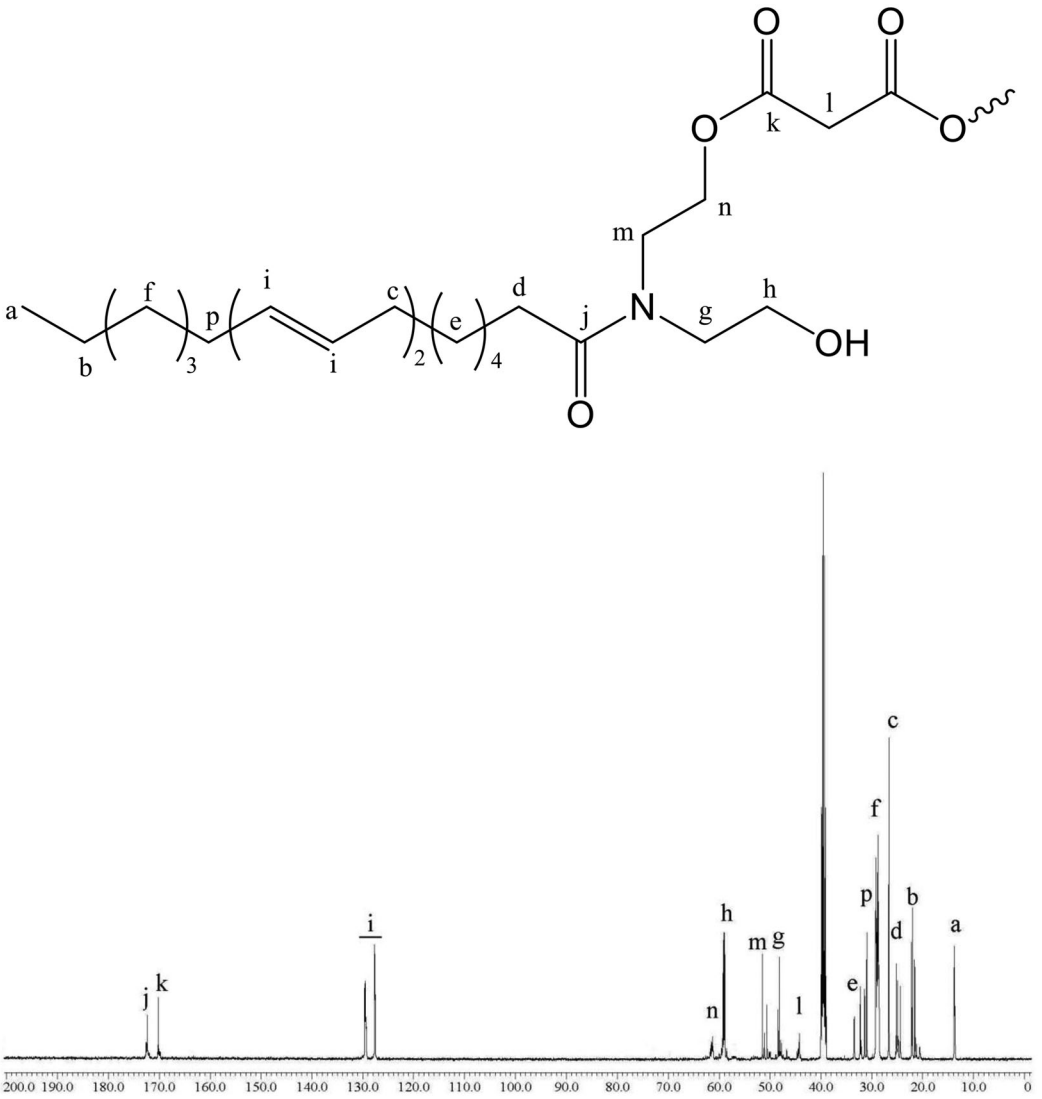

Figure 4. ^{13}C NMR spectra of MPEA.

crosslinked structure that provides an impermeable barrier. The presence of MWCNTs in the organic polymer matrix of PUMEA acts as an additional strong barrier because of the hydrophobic nature of the carbon filler.[47,48]

EIS measurements

The barrier and corrosion properties of PUMEA-0.8-coated mild steel in a 3.5% NaCl solution were measured by EIS at different immersion times The impedance was extracted from the open circuit potential (OCP), potentiostatically maintained during the measurements. The OCP values for the PUMEA-0.8 coating at different immersion times (from 4 to 40 days) are reported in Table 2. From this, it is clear that a longer immersion time resulted in OCP decreasing. The increasingly negative OCP values indicate diffusion of the corrosive electrolyte to the coating/mild steel interface. According to these results, the OCP of PUMEA-0.8 is higher after 4 days

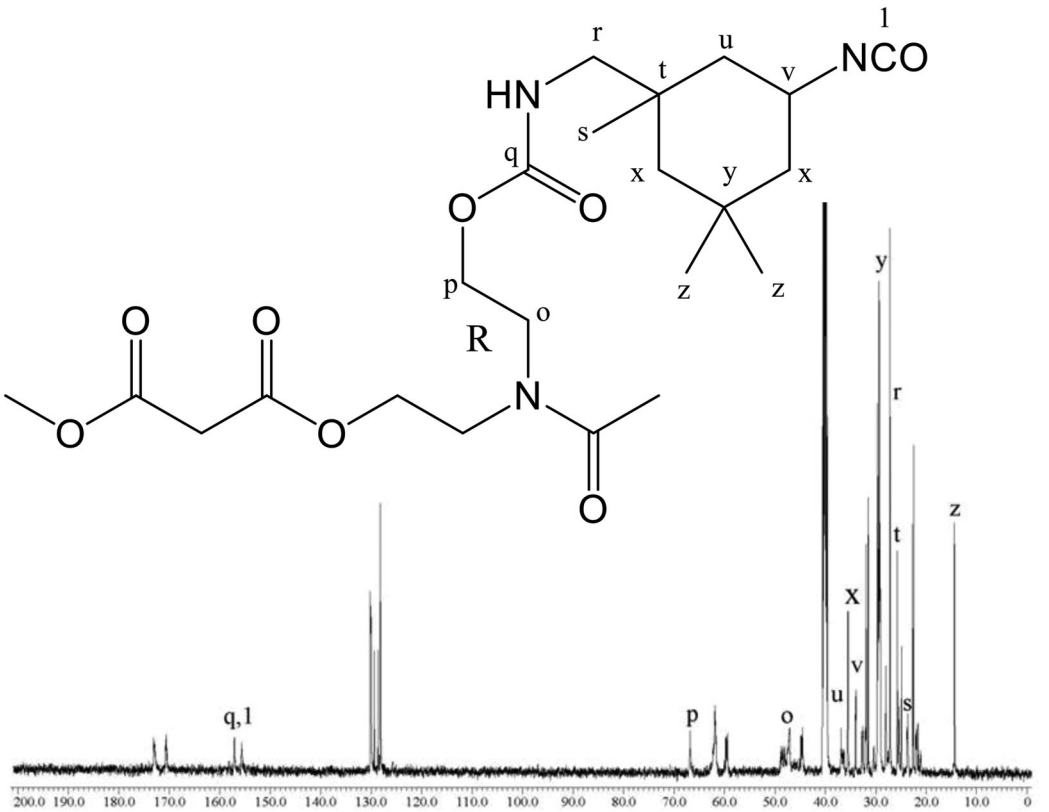

Figure 5. ^{13}C NMR spectra of PUMEA.

than for longer immersion times (8–40 days). This is because of the effective barrier provided by the MWCNTs-modified PUMEA-0.8 film, which deteriorates for increasing immersion times as corrosive ions diffuse toward the mild steel substrate.

The Nyquist and Bode plots of PUMEA-0.8 are displayed in Figures 10 and 11. In the former, only one semicircle is seen, and Warburg impedance can be seen in the latter after 4 days immersion. This suggests that, in these samples, the electrochemical action is mainly controlled by the ionic resistance (barrier effect) of the PUMEA-0.8 coating. As can be seen in Figure 11, the modulus of the PUMEA-0.8 impedance is greater than 10^5 Ω cm^2 following 4 days immersion, and the phase angle is approximately 85° in the high-frequency region. The capacitive performance can be extracted from the Bode phase diagrams of these samples, in the 1–10^5 Hz frequency range. The PUMEA-0.8 coatings display good barrier properties at the primary immersion stage (4 days). When the immersion time increases, the coating barrier deteriorates, as seen from the capacitive performance in the 1−10^2 Hz frequency range of the Bode phase diagrams. This is attributed to the PUMEA-0.8 coating degrading following exposure to the 3.5 wt% NaCl solution up to 40 days, as a consequence of corrosive ions diffusing to the mild steel substrate. Two-time constants can be extracted from the Bode and Nyquist diagrams of PUMEA-0.8, respectively, after 40 days of immersion. This observation illustrates that the PUMEA-0.8 coating degradation results in a decrease of its barrier properties, allowing corrosive ions to reach the substrate. The results show that incorporating MWCNTs in the PUMEA coating improves the barrier.

To investigate the Nyquist plot, the electrical equivalent circuits of Figure 12 were used to model the impedance. The parameters corresponding to the circuits used to fit the experimental data are shown in Table 2, where OCP, R_s, R_{ct}, C_c, and Y_0 are the open circuit potential, solution resistance, charge transfer resistance, coating capacitance, and Warburg of PUMEA-0.8 coating,

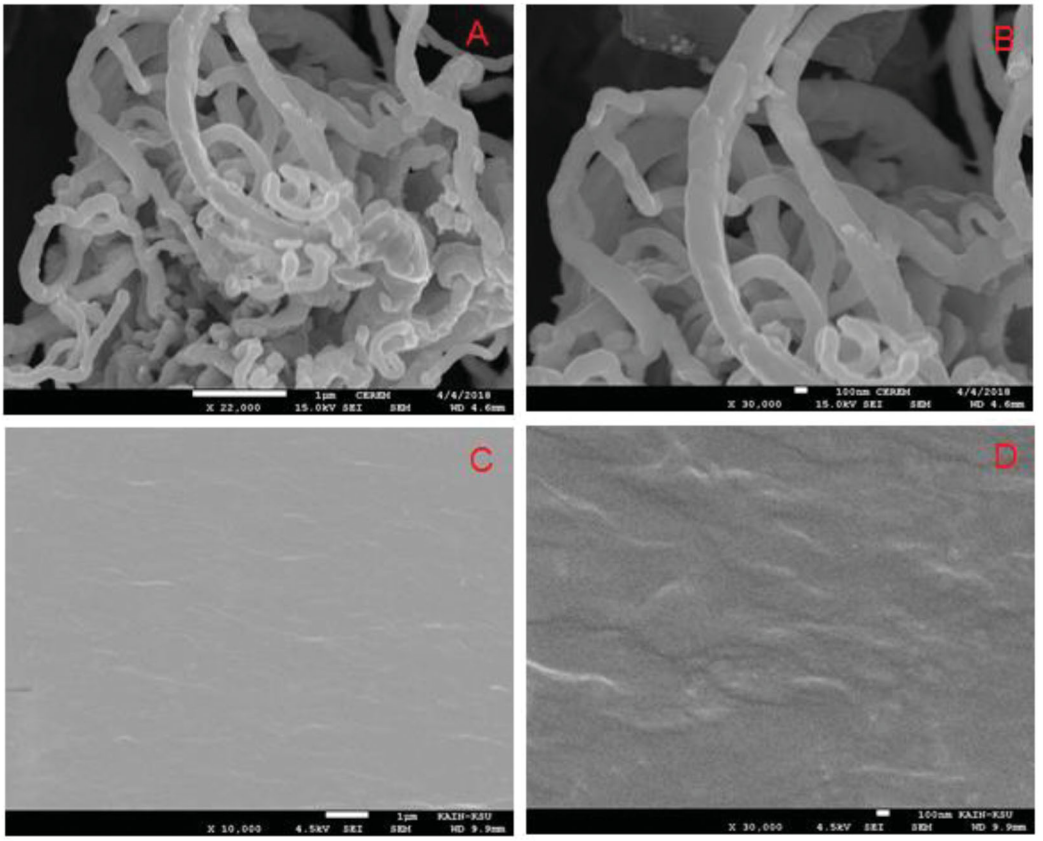

Figure 6. FE SEM images (and size) of (A) MWCNTs (1 μm), (B) MWCNTs (100 nm), (C) PUMEA-0.8 (1 μm), and (D) PUMEA-0.8 (100 nm).

respectively. The values of the impedance at low and high frequency correspond to coating resistance and coating capacitance, respectively. It can be seen from Figure 10 and Table 2 that the frequency range decreases as the immersion time increases, indicating a continuous diffusion of corrosive ions into the PUMEA-0.8 coating. It is clear from these results that the incorporation of MWCNTs into the PUMEA-0.8 coating provides a strengthened and anticorrosive barrier. The plot of the PUMEA-0.8 impedance after 40 days immersion indicates that corrosive ions penetrate the coating; thus, the shielding properties of this importantly deteriorated. The Warburg constant, which can be extracted from the Nyquist plot, indicates that the diffusion current played a significant role in electrochemical corrosion route and that the corrosive ions penetrated the coating and reached the metal substrate. The results of Table 2 indicate that the MWCNTs considerably improved the corrosion protection properties of PUMEA, filling the voids and pores of the polymer matrix where corrosion of the coating can initiate. Another important parameter to evaluate the corrosion protection properties of the PUMEA-0.8 coating is the frequency at 45° phase angle in Bode plots. This is related to the microscopic delaminated parts of the coating.[45–51]

Thermal analysis

The TGA thermograms of the PUMEA and PUMEA-0.8 nanocomposite coatings are shown in Figure 13. A 5% weight loss related to trapped solvent is observed at 275 °C and 267 °C, respectively, and the 13% weight loss respectively measured at 322 °C and 445 °C is associated with

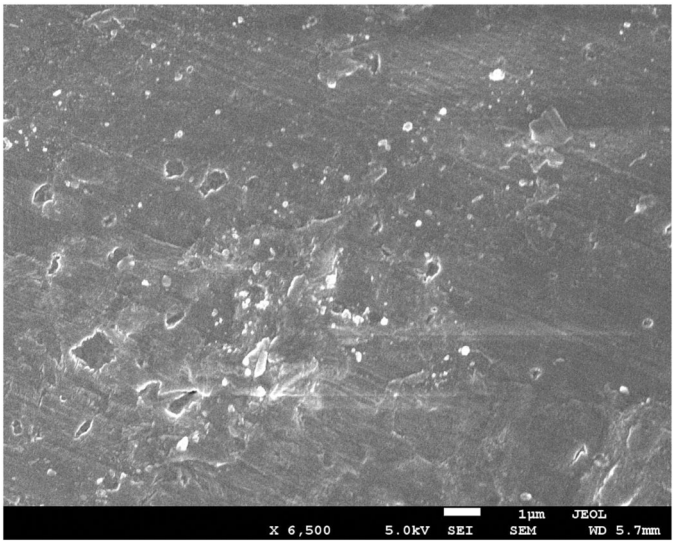

Figure 7. SEM micrograph of PUMEA-0.8 after immersion in 3.5 wt. % NaCl solution.

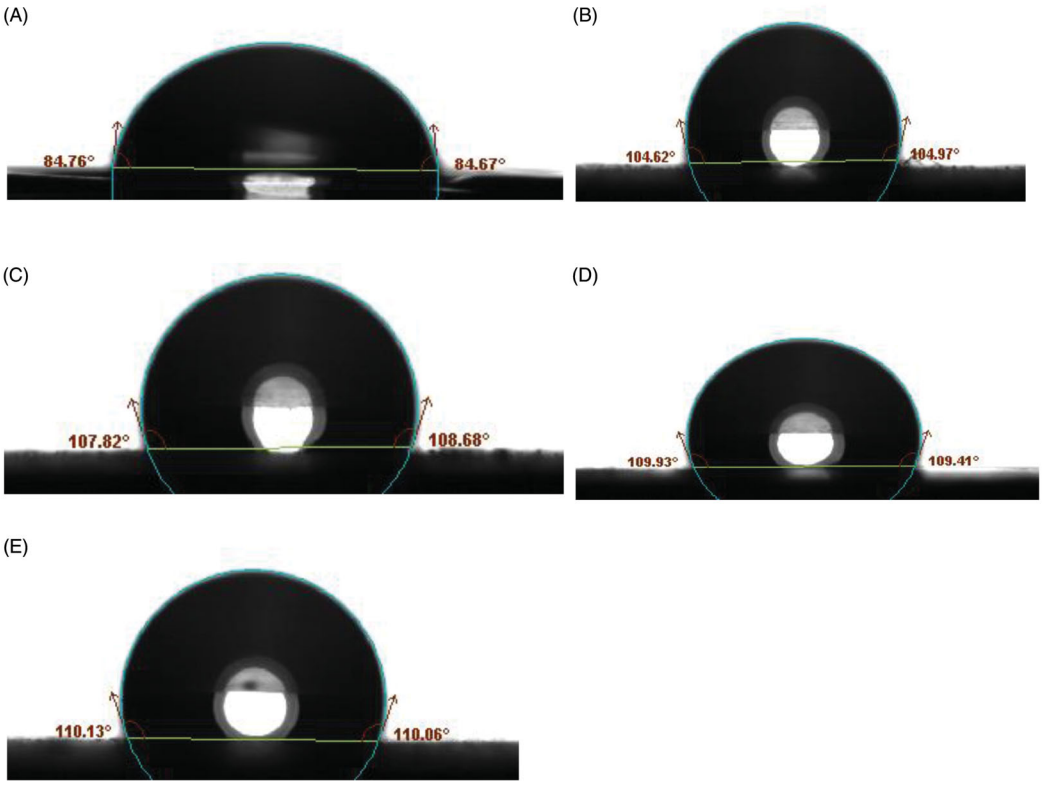

Figure 8. Images of a water drop on the surface of (A) PUMEA, (B) PUMEA-0.4, (C) PUMEA-0.6, (D) PUMEA-0.8, and (E) PUMEA-1.00.

thermal degradation. The DTG thermograms of PUMEA and PUMEA-0.8 shown in Figure 14 display two decomposition steps. The first decomposition peak in PUMEA is centered at 322 °C, ranging between 212 °C and 381 °C. The peak in this range is related to the 13% weight loss of

Table 1. Electrochemical parameters calculated from polarization measurements PUMEA-0.8 coated mild steel in 3.5% NaCl solution for 4–40 days at room temperature.

Immersion time (days)	Corrosion potential E_{corr} (V)	Corrosion current density, I_{corr} (A/cm^2)	Corrosion rate (mm/year)	Polarization resistance (kΩ)
4	−0.25702	6.554E-08	7.616E-04	3.976E + 02
8	−0.27679	1.450E-07	1.648E-03	1.798E + 02
12	−0.34255	1.928E-07	2.240E-03	1.352E + 02
16	−0.36044	2.171E-07	2.522E-03	1.201E + 02
20	−0.42746	2.801E-07	3.255E-03	93.019
24	−0.49759	4.281E-07	4.974E-03	60.863
28	−0.51829	5.189E-07	6.030E-03	50.212
32	−0.54027	6.940E-07	8.064E-03	37.548
36	−0.56988	1.002E-06	1.165E-02	25.998
40	−0.59338	1.166E-06	1.355E-02	22.344

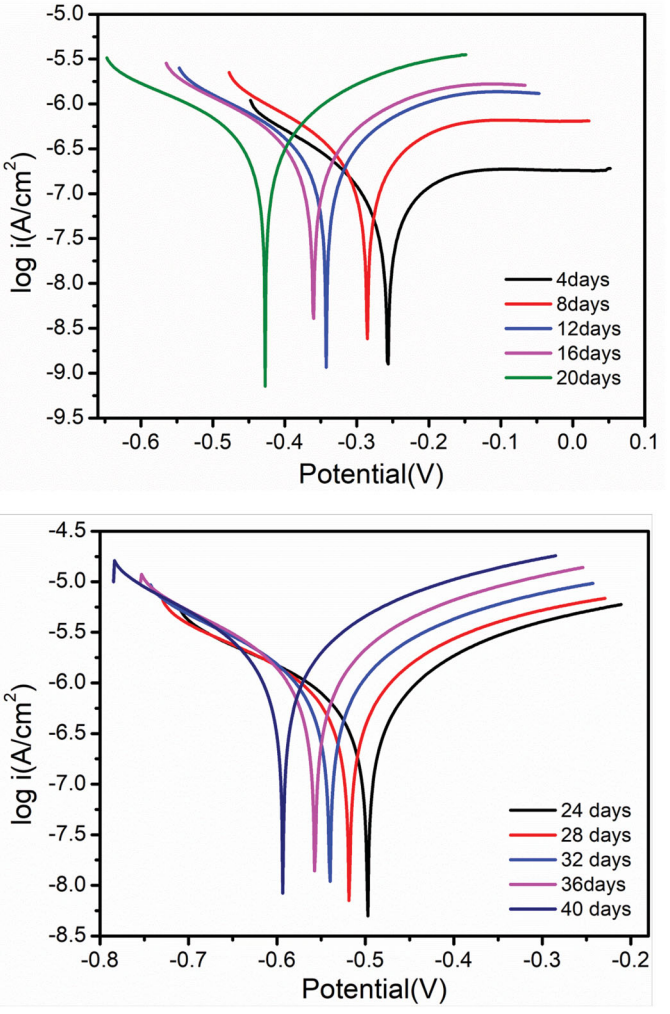

Figure 9. Potentiodynamic polarization plots of the PUMEA-0.8 composite coating after immersion in 3.5 wt% NaCl solution for 40 days.

the TGA thermogram. For PUMEA-0.8, the first decomposition peak is centered at 324 °C and ranges between 220 °C and 385 °C. The second decomposition peak is centered at 476 °C, extending from 381 °C to 550 °C, for PUMEA, and at 490 °C for PUMEA-0.8, extending from 385 °C to

Table 2. The electrochemical parameters observed from impedance data of the PUMEA-0.8 coatings with immersed in 3.5 wt% NaCl solution for 4 to 40 days at room temperature.

Immersion time (days)	OCP (V)	Solution resistance, R_s (kΩ)	Coating capacitance, C_c (pF)	Charge transfer resistance, R_{ct} (kΩ)	Warburg impedance, Y_0 (nmho*s○(1/2))
4	0.058	1.27	93.9	575	186
8	−0.065	3.78	92.9	345	310
12	−0.216	7.29	102	109	11.2
16	−0.223	7.36	120	75.3	19.3
20	−0.228	7.50	140	68.6	122
24	−0.272	7.67	181	49.5	209
28	−0.310	7.76	158	62.2	145
32	−0.461	6.17	221	26.7	297
36	−0.483	5.73	245	21.6	365
40	−0.494	4.96	340	13.4	426

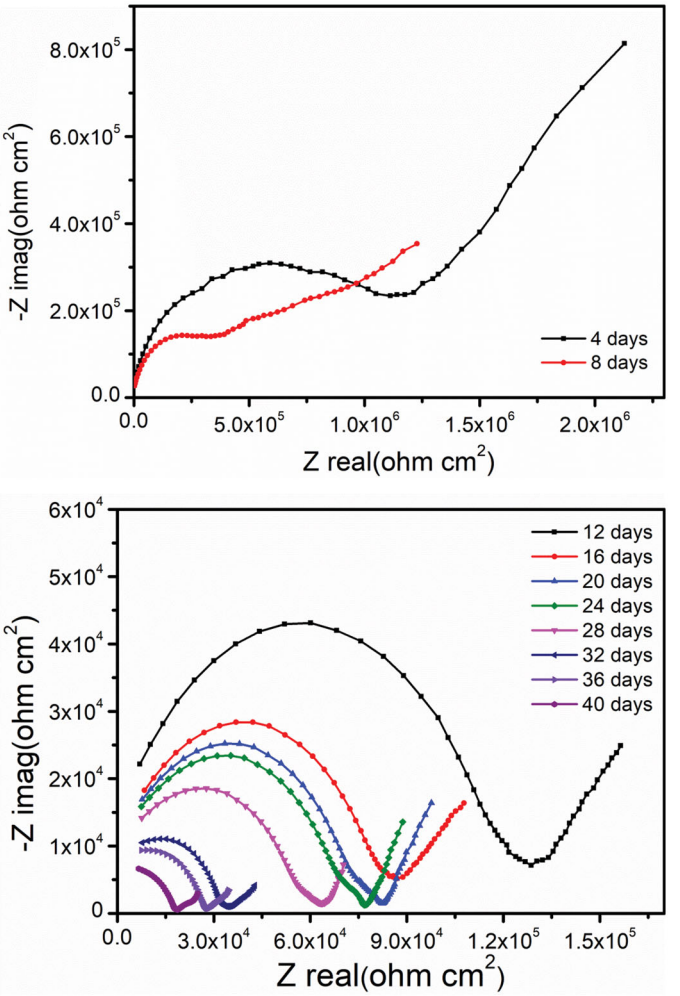

Figure 10. Nyquist plots of the PUMEA-0.8 composite coating after immersion in 3.5 wt.% NaCl solution for 40 days.

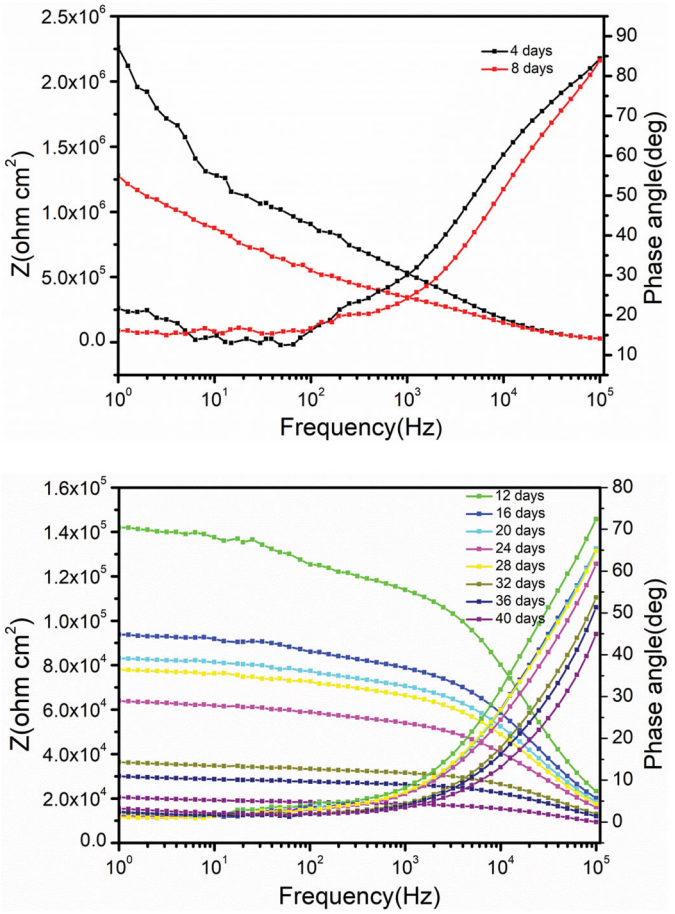

Figure 11. Bode and phase diagrams of the PUMEA-0.8 composite coating after immersion in 3.5 wt% NaCl solution for 40 days.

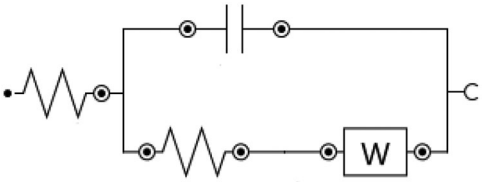

Figure 12. Proposed equivalent circuit to simulate and fit the EIS measurements.

557 °C. The first and second decomposition peaks are related to the decomposition of urethane and the bonding of ester and amide, respectively; the shift of the PUMEA-0.8 peaks is due to the introduction of MWCNTs and their strong interaction with the polymeric chain.

The DSC thermograms of PUMEA and PUMEA-0.8 are shown in Figure 15. PUMEA displays an endothermic peak starting at 85 °C and ending at 244 °C, centered at 222 °C, and a second peak ranging from 245 °C to 384 °C, centered at 271 °C. In PUMEA-0.8, the first endotherm starts at 87 °C and ends at 250 °C, with its center at 229 °C, and the second extends from 247 °C to 386 °C, centering at 275 °C, respectively. These peaks can be attributed to the onset of PUMEA/PUMEA-0.8 melting, followed by decomposition of the polymeric chain, as derived from the TGA thermogram beyond this temperature.

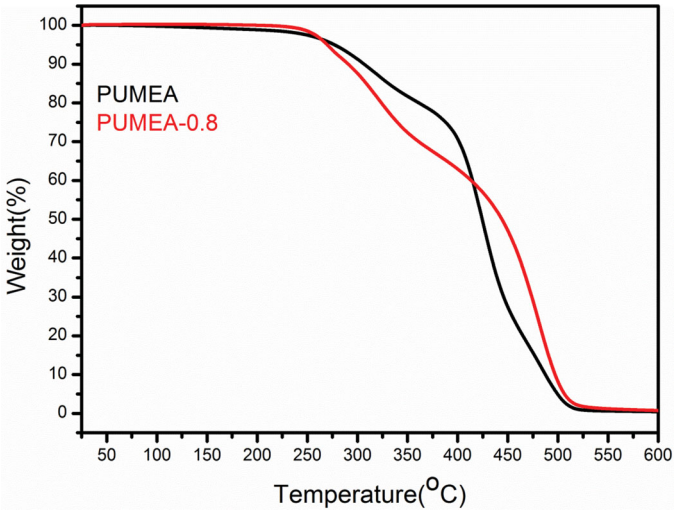

Figure 13. TGA thermogram of PUMEA and PUMEA-0.8.

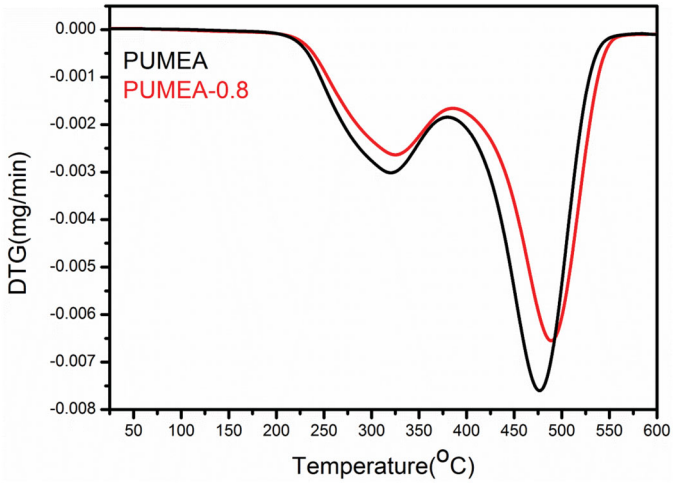

Figure 14. DTG thermogram of PUMEA and PUMEA-0.8.

Conclusion

Natural corn oil-derived PUMEA/MWCNTs composites were successfully synthesized. From this study, it is concluded that the PUMEA-0.8 resin provides the best coating effectiveness among those prepared and that the physico-mechanical properties deteriorate when increasing the content of MWCNTs further. The PUMEA-0.8 resin displays good adhesion, gloss, and resistance to corrosion in a 3.5 wt% NaCl solution up to 32 days. We observed that the 0.8 wt% MWCNTs of the synthesized PUMEA-0.8 composite coating were uniformly dispersed in the PUMEA matrix, and we demonstrated by contact angle, EIS, and polarization measurements that this composite effectively protects the mild steel substrate, being that its barrier properties were enhanced with respect to common polyesteramide coatings. Additionally, the PUMEA-0.8 coating can be safely used up to 250 °C.

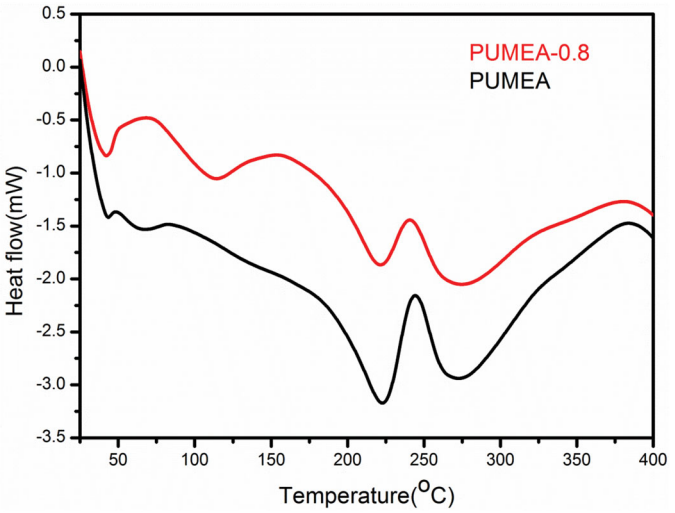

Figure 15. DSC thermogram of PUMEA and PUMEA-0.8.

Funding

The authors are grateful to be the Researchers supporting Project number [RSP-2020/113], King Saud University, Riyadh, Saudi Arabia for the support.

ORCID

Manawwer Alam http://orcid.org/0000-0001-9540-8532

References

[1] Alam, J., M. Alam, M. Raja, Z. Abduljaleel, and L. A. Dass. 2014. MWCNTs-reinforced epoxidized linseed oil plasticized polylactic acid nanocomposite and its electroactive shape memory behaviour. *Int. J. Mol. Sci.* 15:19924–19937. doi:10.3390/ijms151119924

[2] Bhat, S. I., and S. Ahmad. 2018. Castor oil-TiO_2 hyperbranched poly (ester amide) nanocomposite: a sustainable, green precursor-based anticorrosive nanocomposite coatings. *Prog. Org. Coat* 123:326–336. doi:10.1016/j.porgcoat.2018.06.010

[3] Chattopadhyay, D. K., and K. V. S. N. Raju. 2007. Structural engineering of polyurethane coatings for high performance applications. *Prog. Polym. Sci.* 32:352–418. doi:10.1016/j.progpolymsci.2006.05.003

[4] Xu, Y., Z. Petrovic, S. Das, and G. L. Wilkes. 2008. Morphology and properties of thermoplastic polyurethane with dangling chain in ricinoleate-based soft segment. *Polymer* 49:4248–4258. doi:10.1016/j.polymer.2008.07.027

[5] Emamgholizadeh, A., A. Omrani, A. A. Rostami, and A. Rostami. 2015. Corrosion protection of steel 316 using coatings based on epoxy and poly p-phenylendiamine–hen_2 nanocomposite. *Chem. Eng. Commun.* 202:1389–1396. doi:10.1080/00986445.2014.938807

[6] Sharmin, E., O. Rahman, F. Zafar, D. Akram, M. Alam, and S. Ahmad. 2015. Linseed oil polyol/ZnO bionanocomposite towards mechanically robust, thermally stable, hydrophobic coatings: a novel synergistic approach utilising a sustainable resource. *RSC Adv.* 5:47928–47944. doi:10.1039/C5RA03262H

[7] Sharmin, E., F. Zafar, D. Akram, M. Alam, and S. Ahmad. 2015. Recent advances in vegetable oils based environment friendly coatings: a review. *Ind. Crops. Prod.* 76:215–229. doi:10.1016/j.indcrop.2015.06.022

[8] Mannari, V. M., and J. L. Massingill. 2006. Two-component high-solid polyurethane coating system based on soy polyols. *J. Coat. Technol. Res.* 3:151–157. doi:10.1007/s11998-006-0018-1

[9] Ducruet, N., L. Delmotte, G. Schrodj, F. Stankiewicz, N. Desgardin, M.-F. Vallat, and B. Haidar. 2013. Evaluation of hydroxyl terminated polybutadiene-isophoronediisocyanate gel formation during crosslinking process. *J. Appl. Polym. Sci.* 128:436–443. doi:10.1002/app.38194

[10] Khan, S., S. Masood, K. Siddiqui, M. Alam, F. Zafar, Q. M. R. Haque, and N. Nishat. 2018. Utilization of renewable waste material for the sustainable development of thermally stable and biologically active

aliphatic amine modified cardanol (phenolic lipid)-formaldehyde free standing films. *J. Cleaner Prod.* 196: 1644–1656. doi:10.1016/j.jclepro.2018.06.081

[11] Alam, M., N. M. Alandis, E. Sharmin, F. Zafar, and M. A. Alam. 2016. Anticorrosive properties of olive oil polyurethanamide/ZnO biocomposite coatings. *Korean J. Chem. Eng.* 33:1736–1742. doi:10.1007/s11814-016-0009-6

[12] Alam, M., N. M. Alandis, F. Zafar, E. Sharmin, and Y. M. Al-Mohammadi. 2018. Polyurethane-TiO_2 nanocomposite coatings from sunflower-oil-based amide diol as soft segment. *J. Macromol. Sci. A.* 55:698–708. doi:10.1080/10601325.2018.1526638

[13] Tsujimoto, T., H. Uyama, and S. Kobayashi. 2003. Green nanocomposites from renewable resources: biodegradable plant oil-silica hybrid coatings. *Macromol. Rapid Commun.* 24:711–714. doi:10.1002/marc.200350015

[14] Alam, M., N. M. Alandis, and N. Ahmad. 2017. Development of poly(urethane-ester)amide from corn oil and their anticorrosive studies. *Int. J. Polym. Anal. Charact.* 22:281–293. doi:10.1080/1023666X.2017.1287847

[15] Alam, M., N. M. Alandis, E. Sharmin, N. Ahmad, F. M. Husain, and A. Khan. 2020. Mechanically strong, hydrophobic, antimicrobial, and corrosion protective polyesteramide nanocomposite coatings from leucaena leucocephala oil: a sustainable resource. *ACS Omega* 5:30383–30394. doi:10.1021/acsomega.0c03333

[16] Bakshi, M. I., and S. Ahmad. 2020. In-situ synthesis of synergistically active ceria doped polypyrrole oleo-polyesteramide hybrid nanocomposite coatings: corrosion protection and flame retardancy behavior. *Prog. Org. Coat* 147:105778. doi:10.1016/j.porgcoat.2020.105778

[17] Pourhashem, S., M. R. Vaezi, A. Rashidi, and M. R. Bagherzadeh. 2017. Exploring corrosion protection properties of solvent based epoxy-graphene oxide nanocomposite coatings on mild steel. *Corros. Sci.* 115: 78–92. doi:10.1016/j.corsci.2016.11.008

[18] Pourhashem, S., M. R. Vaezi, and A. Rashidi. 2017. Investigating the effect of SiO_2-graphene oxide hybrid as inorganic nanofiller on corrosion protection properties of epoxy coatings. *Surf. Coat Technol.* 311: 282–294. doi:10.1016/j.surfcoat.2017.01.013

[19] Li, W., H. Tian, and B. Hou. 2012. Corrosion performance of epoxy coatings modified by nanoparticulate SiO_2. *Mater. Corros.* 63:44–53. doi:10.1002/maco.200905620

[20] Jamed, M. J., A. A. Alanezi, and Q. F. Alsalhy. 2019. Effects of embedding functionalized multiwalled carbon nanotubes and alumina on the direct contact poly(vinylidene fluoride-cohexafluoropropylene) membrane distillation performance. *Chem. Eng. Commun.* 206:1035–1057. doi:10.1080/00986445.2018.1542302

[21] Yabuki, A., W. Urushihara, J. Kinugasa, and K. Sugano. 2010. Self-healing properties of TiO_2 particle–polymer composite coatings for protection of aluminum alloys against corrosion in seawater. *Mater. Corros.* 61:1–6.

[22] Fihri, A., D. Abdullatif, H. B. Saad, R. Mahfouz, H. Al-Baidary, and M. Bouhrara. 2019. Decorated fibrous silica epoxy coating exhibiting anti-corrosion properties. *Prog. Org. Coat* 127:110–116. doi:10.1016/j.porgcoat.2018.09.025

[23] Yarahmadi, E., K. Didehban, M. G. Sari, M. R. Saeb, M. Shabanian, F. Aryanasa, P. Zarrintaj, S. M. R. Paran, M. Mozafari, M. Rallini, and D. Puglia. 2018. Development and curing potential of epoxy/starch functionalized graphene oxide nanocomposite coatings. *Prog. Org. Coat* 119:194–202. doi:10.1016/j.porgcoat.2018.03.001

[24] Zhu, K., X. Li, H. Wang, J. Li, and G. Fei. 2017. Electrochemical and anti-corrosion behaviors of water dispersible graphene/acrylic modified alkyd resin latex composites coated carbon steel. *J. Appl. Polym. Sci.* 134:44445.

[25] Esposito, L. H., J. A. Ramos, and G. Kortaberria. 2014. Dispersion of carbon nanotubes in nanostructured epoxy systems for coating application. *Prog. Org. Coat* 77:1452–1458. doi:10.1016/j.porgcoat.2014.05.001

[26] Abdolmaleki, A., S. Mallakpour, and M. Rostami. 2015. Development of carboxylated multi-walled carbon nanotubes reinforced potentially biodegradable poly(amideamideled carbon nantrimellitylimido-S-valine matrixes: preparation, processing, and thermal properties. *Prog. Org. Coat* 80:71–76. doi:10.1016/j.porgcoat.2014.11.019

[27] Takassi, M. A., A. Zadehnazari, A. Farhadi, and S. Mallakpour. 2015. Highly stable polyimide composite films based on 1,2,4-triazole ring reinforced with multi-walled carbon nanotubes: study on thermal, mechanical, and morphological properties. *Prog. Org. Coat* 80:142–149. doi:10.1016/j.porgcoat.2014.12.001

[28] Zhang, L., H. Wu, Z. Zheng, H. He, M. Wei, and X. Huang. 2019. Fabrication of graphene oxide/multi-walled carbon nanotube/urushiol formaldehyde polymer composite coatings and evaluation of their physicomechanical properties and corrosion resistance. *Prog. Org. Coat* 127:131–139. doi:10.1016/j.porgcoat.2018.10.026

[29] Kermani, H. H., V. Mottaghitalab, M. Mokhtary, and A. A. Dakhel. 2020. Morphological, rheological, and mechanical properties of ethylene propylene diene monomer/carboxylated styrene-butadiene rubber/multi-wall carbon nanotube nanocomposites. *Int. J. Polym. Anal. Charact.* 25:479–498. doi.org/10.1080/1023666X.2020.1807681

[30] Zhang, H., H. Li, L. Liu, Y. Zhang, X. Zhang, and Z. Li. 2018. The potential role of malonic acid in the atmospheric sulfuric acid – ammonia clusters formation. *Chemosphere* 203:26–33. doi:10.1016/j.chemosphere.2018.03.154

[31] Apelblat, A., and E. Manzurola. 2016. Volumetric properties of aqueous solutions of malonic acid. *J. Chem. Thermodynamics* 102:63–67. doi:10.1016/j.jct.2016.06.023

[32] Zhu, H. L., and Y. Q. Zheng. 2012. The synthesis, crystal structures, and thermal properties of a new Zn(II) coordination polymer with malonic acid. *Synt. React. Inor. Metal Org. Nano Metal Chem.* 42: 736–740. doi:10.1080/15533174.2011.615073

[33] Ghosh, T., and N. Karak. 2020. Mechanically robust hydrophobic interpenetrating polymer network-based nanocomposite of hyperbranched polyurethane and polystyrene as an effective anticorrosive coating. *New J. Chem.* 44:5980–5994. doi:10.1039/D0NJ00322K

[34] Zheng, Y. Q., and H. Z. Xie. 2004. Two malonato coordination polymers: syntheses and crystal structures of $M(H_2O)_2(C_3H_2O_4)$ with M = CO and Ni, $C_3H_4O_4$ = malonic acid. *J. Coord. Chem.* 57:1537–1543. doi: 10.1080/0095897052000273509

[35] Ramezanzadeh, B., S. Niroumandrad, A. Ahmadi, M. Mahdavian, and M. H. M. Moghadam. 2016. Enhancement of barrier and corrosion protection performance of an epoxy coating through wet transfer of amino functionalized graphene oxide. *Corros. Sci.* 103:283–304. doi:10.1016/j.corsci.2015.11.033

[36] Vogelsang, J., and W. Strunz. 2001. Electrochemical investigations of organic, corrosion protective barrier coatings - limiting factors of small signal perturbation techniques. *Mater. Corros.* 52:462–469. doi:10.1002/1521-4176(200106)52:6<462::AID-MACO462>3.0.CO;2-K

[37] Samuel, P. S., R. Kumar, D. S. R. Smart, and S. J. Alexis. 2017. Corrosion behaviour of aluminium metal matrix reinforced with multi-wall carbon nanotube. *J. Asian Ceramic Soc.* 5:71–75.

[38] Jiang, Y., S. Y. Zhang, X. L. Zhang, and T. Zhang. 2018. Improving the performance of UV-curable coatings with carbon nanomaterials. *eXPRESS Polym. Lett.* 12:628–639. doi:10.3144/expresspolymlett.2018.53

[39] Parhizkar, N., T. Shahrabi, and B. Ramezanzadeh. 2017. A new approach for enhancement of the corrosion protection properties and interfacial adhesion bonds between the epoxy coating and steel substrate through surface treatment by covalently modified amino functionalized graphene oxide film. *Corros. Sci.* 123:55–75. doi:10.1016/j.corsci.2017.04.011

[40] Sabirneeza, A. A. F., S. Subhashini, and R. Rajalakshmi. 2013. Water soluble conducting polymer composite of polyvinyl alcohol and leucine: an effective acid corrosion inhibitor for mild steel. *Mater. Corros.* 64: 74–82. doi:10.1002/maco.201106096

[41] Alam, M., and N. M. Alandis. 2014. Corn oil based poly(ether amide urethane) coating material—synthesis, characterization and coating properties. *Ind. Crops Prod.* 57:17–28. doi:10.1016/j.indcrop.2014.03.023

[42] Wahab, R., S. G. Ansari, Y. S. Kim, T. R. Mohanty, I. H. Hwang, and H.-S. Shin. 2009. Immobilization of DNA on nano-hydroxyapatite and their interaction with carbon nanotubes. *Synth. Met.* 159:238–245. doi: 10.1016/j.synthmet.2008.09.016

[43] Dolatzadeh, F., M. M. Jalili, and S. Moradian. 2013. Influence of various loadings of hydrophilic or hydrophobic silica nanoparticles on water uptake and porosity of a polyurethane coating. *Mater. Corros.* 64: 609–617. doi:10.1002/maco.201106381

[44] Alam, M., D. Akram, E. Sharmin, F. Zafar, and S. Ahmad. 2014b. Vegetable oil based eco-friendly coating materials: a review article. *Arab. J. Chem.* 7:469–479. doi:10.1016/j.arabjc.2013.12.023

[45] Ye, Y., D. Zhang, J. Li, T. Liu, J. Pu, H. Zhao, and L. Wang. 2019. One-step synthesis of superhydrophobic polyhedral oligomeric silsesquioxane-graphene oxide and its application in anti-corrosion and antiwear fields. *Corros. Sci.* 147:9–21. doi:10.1016/j.corsci.2018.10.034

[46] Gergely, A., Z. Paszti, I. Bertoti, T. Torok, E. Pfeifer, and E. Kalman. 2013. Novel zinc-rich epoxy paint coatings with hydrated alumina and carbon nanotubes supported polypyrrole for corrosion protection of low carbon steel part I: inhibitor particles and their dispersions. *Mater. Corros.* 64:1082–1090. doi:10.1002/maco.201206706

[47] Hamer, W. J., L. Koene, and J. H. W. de Wit. 2004. Formation and electrochemical behaviour of poly(pyrrole) coatings on steel substrates. *Mater. Corros.* 55:653–658. doi:10.1002/maco.200303778

[48] Iribarren, J. I., E. Armelin, F. Liesa, J. Casanovas, and C. Aleman. 2006. On the use of conducting polymers to improve the resistance against corrosion of paints based on polyurethane resins. *Mater. Corros.* 57: 683–688. doi:10.1002/maco.200503952

[49] Darowicki, K., and S. Janicki. 2000. Electrochemical investigations of modified polymeric composites. *Mater. Corros.* 51:835–840. doi:10.1002/1521-4176(200012)51:12<835::AID-MACO835>3.0.CO;2-3

[50] Hou, W. P., Y. Liu, Z. Y. Ge, and W. Y. Zhao. 2013. Comparison study on anticorrosion performances of the epoxy coatings with two different nano-polyanilines for Q235 steel. *Mater. Corros.* 64:960–968. doi:10.1002/maco.201206862

[51] Bhuvaneshwari, B., A. Selvaraj, N. R. Iyer, and L. Ravikumar. 2015. Electrochemical investigations on the performance of newly synthesized azomethine polyester on rebar corrosion. *Mater. Corros.* 66:387–395. doi: 10.1002/maco.201307472